Design and Control of an Omnidirectional Aerial Robot with a Miniaturized Haptic Joystick for Physical Interaction

Julien Mellet*[1], Andrea Berra*[2], Salvatore Marcellini[4], Miguel Ángel Trujillo Soto[2], Guillermo Heredia[3], Fabio Ruggiero[1], Vincenzo Lippiello[1]

***Abstract*— Fully actuated aerial robots have shown superiority in Aerial Physical Interaction (APhI) in recent years. This work presents a minimal setup for aerial telemanipulation, improving accessibility to such technologies. The design and control of a 6-Degrees of Freedom (DoF) joystick with 4-DoF haptic feedback are detailed. It is the first haptic device with standard Remote Controller (RC) form factor for APhI. Miniaturizing the haptic device adds sense of touch to RC, enhancing physical awareness. The goal is to provide operators with an extra sense—beyond vision and sound—to support safe APhI. To the best of the authors' knowledge, this is the first 6-DoF aerial teleoperation system capable of decoupling single-axis input commands. The proposed robot hardware design reduces number of components, aiming for easier maintenance and improved force and thrust-to-weight ratios. Open-source physics-based simulation and successful early flight tests highlight the tool's promise for future APhI applications.**

This project has received funding from the European Union's Horizon 2020 research and innovation program under the Marie Skłodowska-Curie grant agreement No 953454.

This project has also received funding from the AI-DROW project, in the frame of the PRIN 2022 research program, grant n. 2022BYSBYX, funded by the European Union Next-Generation EU.

[1]PRISMA Lab, Department of Electrical Engineering and Information Technology, University of Naples Federico II Naples, Italy.

[2]CATEC, Advanced Center for Aerospace Technologies, Seville, Spain.

[3]GRVC, Robotics, Vision and Control Group School of Engineering, University of Seville Seville, Spain.

[4]Leonardo Innovation Labs, Leonardo S.p.A., 00195 Rome, Italy. The research presented herein was conducted while the author was enrolled at PRISMA Lab. Leonardo S.p.A. was not involved in the development of this article or its content.

*The authors contributed equally

Corresponding Authors' email: julien.mellet@unina.it

I. Introduction

The field of Unmanned Aerial Vehicle (UAV)s has evolved from aeromodelism technologies, leading to the use of 4-DoF radio controllers to pilot most of the multirotor platform. Similarly, ground robots are often operated using gamepad-like controllers. However, with the advent of Omnidirectional Micro Aerial Vehicle (OMAV)s [1], which offer full actuation capabilities for aerial physical interaction (APhI), limitations in current control interfaces are becoming evident. Specifically, there is a shortage of input channels and a lack of tactile feedback to inform the operator during complex maneuvers. Haptic devices, mainly developed for medical purposes [2], could address these limitations. Within the context of aerial robotics [3], integrating force and tactile feedback into conventional controller designs, operators can be better informed about external forces acting on the vehicle, such as wind disturbances or physical interactions with surfaces. Furthermore, optimizing the interface for seamless integration with full-actuation platforms, such as OMAVs, would allow operators to fully exploit the agility and control potential of these vehicles, leading to more stable and responsive flight performance.

This paper seeks to bridge the gap between research on haptic aerial control and industrial inspection by miniaturizing the interface into a conventional joystick device. It presents an open-source telemanipulation system that can be replicated using standardized tools within a unified teleoperation framework. To the best of the author's knowledge,

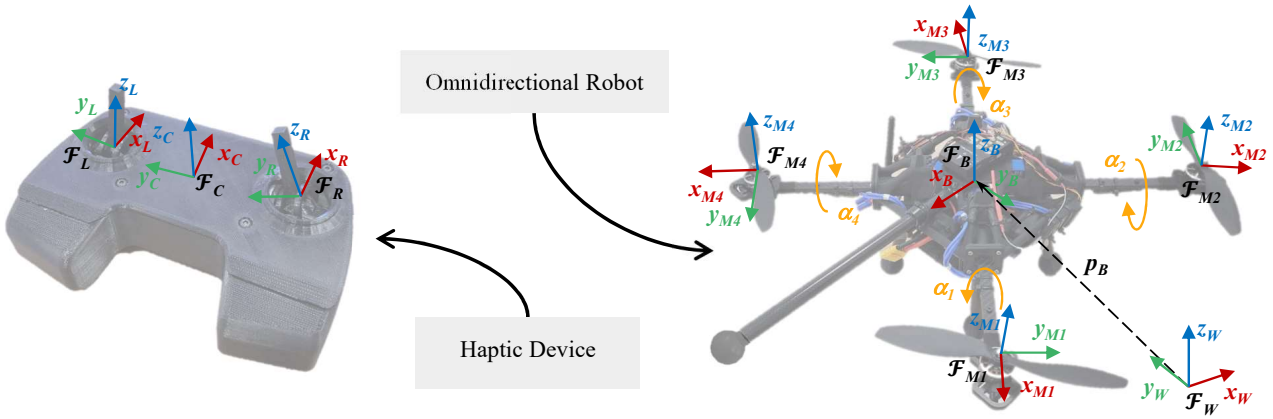

Fig. 1: The telemanipulation system includes the joystick (*left*) and the aerial robot (*right*). The haptic joystick with its frame $\mathcal{F}_C$ and miniaturized force feedback mechanism on the sticks with respective left $\mathcal{F}_L$ and right $\mathcal{F}_R$ frames. The omnidirectional quadrotor with its body frame $\mathcal{F}_B$, in position $\boldsymbol{p}_B$ with respect to the world frame $\mathcal{F}_W$. The four tilting rotor frames $\mathcal{F}_M$ are with $\boldsymbol{z}_M$ pointing up and $\boldsymbol{x}_M$ along the robot arms with α angles around them.

this work is the first to integrate standard RC joysticks with significant force feedback into an operational omnidirectional device.

A. Related Works

Omnidirectional multirotors are mechanically more complex than underactuated multirotors. The integration of rotating mechanisms within the arms significantly increases the system's complexity, as described in platforms introduced in [4], [5]. Additionally, the incorporation of arms designed for contact devices, along with the addition of sensors for tasks such as contact inspection, further complicates the hardware architecture [6]. The increased complexity results in a lower thrust-to-weight ratio and it generally makes these platforms more challenging to maintain and repair in the event of an accident. As a result, omnidirectional aerial robots designed for physical interactions are sophisticated systems that require substantial attention and precision. To mitigate these challenges and ensure safe deployment in real-world applications, physical simulators for omnidirectional drones, such as OmniDrones [7], have been developed to test algorithms prior to flight testing. While OmniDrones provides a flexible platform for simulating free-flight scenarios, its limitations—such as the lack of haptic feedback and the absence of a full flight control system or Software In The Loop (SITL) simulation—restrict its ability to fully replicate real-world behaviors and interactions. It is primarily oriented for free-flight using reinforcement learning, but does not embed a Flight Controller (FC) system or SITL.

Haptics for aerial robots has been applied in various manners [8]–[10]. For bilateral teleoperation [11] of omnidirectional robots, hand-held joysticks, later called Haptic Hand Joystick (HHJ), are commonly used [12], [13]. Unfortunately, these joysticks cannot fully decouple rotational movements from unintended translations [14], severely limiting the applicability of 6-DoF systems. Furthermore, a widespread use of these joysticks would require the retraining of all teleoperators. Although a 3-translational DoF haptic stick has been proposed [15], its lack of force intensity and shows fragility due to its foldable mechanism. Therefore, the origamic foldable mechanism is not suitable for safe deployment because robust force feedback is essential for safe aerial vehicle steering.

Thus, there is a need for a portable, on-site joystick that maintains the familiar RC form factor while enhancing teleoperator performance through haptic augmentation. However, the challenge of effectively mapping 4-DoF inputs to the 6-DoF capabilities of the OMAV remains unresolved. While APhI applications have been successfully demonstrated in recent years, no prior research has managed to deliver a complete aerial telemanipulation system that addresses these challenges and is accessible to the broader community.

B. Contributions

This work proposes and shares a full system for aerial physical interaction in the haptic telemanipulation context that includes the robot with its joystick and simulator. The main contributions include *i)* the simplification and open-sourcing of the hardware design for an omnidirectional aerial robot, including its FC, *ii)* the design features of a compact Haptic Finger Joystick (HFJ) with a standard RC form factor, capable of delivering high-force feedback for enhanced operator immersion, and *iii)* evaluation of the proposed telemanipulation system showing single axis command capability.

II. Omnidirectional Platform

To enable effective APhI, the design of the aerial platform plays a crucial role in ensuring precise 6-DoF control, stability, and efficient wrench generation. The description of the omnidirectional aerial vehicle details the dynamic model, control strategies, and mechanical design to support advanced telemanipulation capabilities, complementing the proposed HFJ control strategy.

A. Model

The omnidirectional multirotor is described by an inertial world frame $\mathcal{F}_W$, where O_W is the origin and $\boldsymbol{x}_W, \boldsymbol{y}_W, \boldsymbol{z}_W$ are unit axes, located at an arbitrary fixed point such that $\boldsymbol{z}_W$ points in the opposite direction of gravity, as illustrated in Fig. 1. The state of the platform is defined in the body frame $\mathcal{F}_B = O_B, \boldsymbol{x}_B, \boldsymbol{y}_B, \boldsymbol{z}_B$, with the origin O_B coinciding with the robot's Center of Mass (CoM), and $\boldsymbol{x}_B$ is oriented toward the end-effector stick. The state of the system is then defined by the position of O_B relative to $\mathcal{F}_W$, illustrated as $\boldsymbol{p}_B \in \mathbb{R}^3$. The attitude of $\mathcal{F}_B$ with respect to $\mathcal{F}_W$ is described by the rotation matrix $\boldsymbol{R}_B^W \in \mathsf{SO}(3)$. From $\boldsymbol{R}_B^W$, we can extract the Euler angles $(\phi_B, \theta_B, \psi_B)$ to express the robot's attitude in $\mathcal{F}_B$ with respect to $\mathcal{F}_W$. In addition, the linear and angular velocities of the body with respect to $\mathcal{F}_W$ are denoted as $\boldsymbol{v}_B \in \mathbb{R}^3$ and $\boldsymbol{\omega}_B \in \mathbb{R}^3$, respectively. Therefore, when expressed in the body-fixed frame $\mathcal{F}_B$, the system dynamic model can be described in Lagrangian form [4], [16]:

$$\boldsymbol{M} \begin{bmatrix} \dot{\boldsymbol{v}}_B \\ \dot{\boldsymbol{\omega}}_B \end{bmatrix} + \boldsymbol{C} \begin{bmatrix} \boldsymbol{v}_B \\ \boldsymbol{\omega}_B \end{bmatrix} + \boldsymbol{g} = \boldsymbol{\tau}_a + \boldsymbol{\tau}_{\text{ext}}, \tag{1}$$

where $\boldsymbol{M}, \boldsymbol{C} \in \mathbb{R}^{6\times6}$ are symmetric positive definite matrix representing the body inertia matrix and he matrices of centrifugal and Coriolis wrench, $\boldsymbol{g} \in \mathbb{R}^{6\times1}$ denotes the gravitational wrench vector, $\boldsymbol{\tau}_{\text{ext}} \in \mathbb{R}^6$ indicates the external wrench acting on the platform and $\boldsymbol{\tau}_a \in \mathbb{R}^6$ defines the wrench command.

B. Control

For a compliant interaction with contact surfaces, the control structure is based on an impedance controller adapted for the omnidirectional multirotor [4]. This implies that we can safely interact with the surfaces. The closed-loop dynamics of the system can then be expressed in the following way:

$$\boldsymbol{M}_v \begin{bmatrix} \dot{\boldsymbol{v}}_B \\ \dot{\boldsymbol{\omega}}_B \end{bmatrix} + \boldsymbol{D}_v \begin{bmatrix} \boldsymbol{e}_v \\ \boldsymbol{e}_\omega \end{bmatrix} + \boldsymbol{K}_v \begin{bmatrix} \boldsymbol{e}_p \\ \boldsymbol{e}_R \end{bmatrix} = \boldsymbol{\tau}_a + \boldsymbol{\tau}_{\text{ext}}, \tag{2}$$

where $\mathbf{M}_v$, $\mathbf{D}_v$, $\mathbf{K}_v \in \mathbb{R}^{6\times6}$ are the virtual inertia, damping, and stiffness matrices, respectively, which are controller parameters, and $\boldsymbol{\tau}_{\text{ext}}$ which defines the external wrench applied on the platform. Further, tracking error terms are defined in $\mathcal{F}_B$, where $\boldsymbol{e}_p$, $\boldsymbol{e}_R$, $\boldsymbol{e}_v$, and $\boldsymbol{e}_\omega$ indicate the position, orientation, linear, and angular velocity errors:

$$\boldsymbol{e}_p = \boldsymbol{R}_B^{W\top}\left(\boldsymbol{p}_B - \boldsymbol{p}_{B,\text{ref}}\right), \tag{3a}$$

$$\boldsymbol{e}_R = \frac{1}{2}\left(\boldsymbol{R}_{B,\text{ref}}^{W\top}\boldsymbol{R}_B^W - \boldsymbol{R}_B^{W\top}\boldsymbol{R}_{B,\text{ref}}^W\right)^\vee, \tag{3b}$$

$$\boldsymbol{e}_v = \boldsymbol{R}_B^{W\top}\left(\boldsymbol{v}_B - \boldsymbol{v}_{B,\text{ref}}\right), \tag{3c}$$

$$\boldsymbol{e}_\omega = \boldsymbol{\omega}_B - \boldsymbol{R}_B^{W\top}\boldsymbol{R}_{B,\text{ref}}^W\boldsymbol{\omega}_{B,ref}, \tag{3d}$$

with $(\cdot)^\vee$ the Vee operator to extract a vector from a skew-symmetric matrix. The reference position and orientation mentioned in Eq. (3), $\boldsymbol{p}_{B,\text{ref}}$ and $\boldsymbol{R}_{B,\text{ref}}^W$, are generated from the haptic device, as detailed in Sec. III.

C. Control allocation

The control allocation problem for an omnidirectional multirotor with tiltable arms consists of finding the optimal rotor speeds $\omega_1, ..., \omega_4$ and, differently from standard multirotors, the optimal tilt-angles $\alpha_1, ..., \alpha_4$ to generate the desired wrench $\boldsymbol{\tau}_a$. This problem has been solved as in [17], where the allocation matrix is formulated to distinctly separate the vertical and lateral forces produced by each rotor. It is essential to account for uncertainties when utilizing cost-effective actuators, such as servomotors, for the actuation of the tiltable arms. Servomotors typically exhibit minimal positioning errors in steady-state conditions; however, when considering the inertia of the propulsion system (motor and propeller), they may experience non-negligible uncertainties in angular velocity, particularly during transient phases. Also, due to the critical coupling between the evolution of the tilt angles and the rotors' speed, even slight mismatches can lead to the generation of a wrench that differs from the intended one. Experiments have shown that this effect can lead to significant uncontrolled platform's behavior. The least significant effect arises from minor positioning errors during transient phases, which can be mitigated through appropriate controller tuning. In contrast, the most pronounced impact of these uncertainties is observed in the yaw angle dynamics, where small tilt angle deviations can induce oscillations and potentially lead to instability. To address this issue, a damping constant has been incorporated into the static allocation matrix $\boldsymbol{A}_s$ proposed in [17], in order to reduce the lateral force required to generate the desired moments

$$A(\phi,i)_s = k_\phi A^l(\psi,i)_s + (1-k_\phi)A^v(\phi,i)_s, \tag{4a}$$

$$A(\theta,i)_s = k_\theta A^l(\psi,i)_s + (1-k_\theta)A^v(\theta,i)_s, \tag{4b}$$

$$A(\psi,i)_s = k_\psi A^l(\psi,i)_s + (1-k_\psi)A^v(\psi,i)_s, \tag{4c}$$

where $(k_\phi, k_\theta, k_\psi) \in [0,1]$ represent the damping coefficients for roll, pitch, and yaw, respectively, while $(A^l(.)_s, A^v(.)_s)$ denote the lateral and vertical force contributions to the mixer. If $k_i > 0$, the corresponding moment is coupled with the tilt angles of the rotors. As experimental results shown in Sec. IV, the robot demonstrated accurate tracking performance, despite the servomotor uncertainties in angular speed.

D. Mechanical Design

We design a quadrotor platform with one DoF per robotic arm, following a similar approach to those presented in [4], [18]. However, in contrast to the proposed platforms, only four arms with a single rotor per arm are employed. Coaxial configurations [4] have been avoided to mitigate potential undesirable aerodynamic interactions, while hexacopter architectures were not considered [18] due to their increased mechanical complexity and larger footprint. Indeed, the choice of a quadrotor may reduce the maximum achievable force and torque in the body frame compared to other architectures, it provides advantages such as a reduced number of components and smaller footprint. Overall, the structure of the platform is composed of a robot chassis to which the four arms are attached. The robot chassis design has been optimized using generative design methods [19] to minimize weight and footprint while maintaining rigidity under internal stresses. The optimization process explicitly models the distribution of internal forces and mechanical constraints within each component, which allows for a systematic exploration of multiple design alternatives [19]. Further, each arm is constructed by directly linking a motor to two sheets of carbon fiber, with a revolute joint formed by two coupling parts that connect the carbon fiber arm to the main chassis. Finally, a 10-inch propeller is attached to each rotor, for a compact design and good efficiency design. The details of the platform's main components and their corresponding weights are summarized in Table I, and the complete assembly information is available on GitHub[1] repo. With the proposed design, we then evaluate the force and

Component	Name	Weight [g]
Servos	SPT4412LV	260
Rotors	XING2 2809 1250KV	243
Battery	4s 6000mAh	600
Companion Computer	Lattepanda	55
Flight Controller	Pixhawk 6C	16
Frame	Generative Designed Custom	1340

TABLE I: Omnidirectional quadrotor components and weights. The total weight at take-off is 2.1 kg.

torque generation of the platform, by sending a set of forces and torque values to the mixer proposed in Sec. II-C. The set of feasible wrenches is constrained by the system's physical limitations, namely a maximum servo tilt angle of π radians and the maximum rotor speed allowed by the selected motors (Fig. 2). These constraints define the wrench envelope, from which we observe that the platform is capable of generating up to 50 N along $\boldsymbol{z}_B$ and up to 30 N along $\boldsymbol{x}_B$ and $\boldsymbol{y}_B$ (Fig. 2a). In terms of torque, the system can produce a maximum torque of 5.8 Nm on $\boldsymbol{x}_B$ and $\boldsymbol{y}_B$ and 10.3 Nm on $\boldsymbol{z}_B$ (Fig. 2b). We also evaluate the thrust efficiency η_f and torque efficiency η_m of the generated envelope defined in

[1] https://github.com/tilties2/Haptic-OmniQuad.git

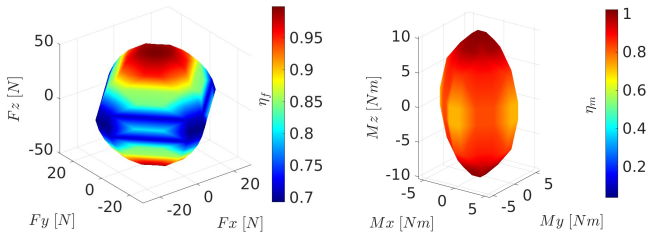

(a) Force Envelope (b) Torque Envelope

Fig. 2: Force and torque representation with respectively thrust efficiency index η_f and torque efficiency index η_m. Feasible values are achieved with servo angles $\alpha \in [-\pi, \pi]$ and rotor speeds within the maximum operational range, $\omega \in [0, 2199.17]$rad/s.

[20]. They quantify the internal forces and torques dissipated in overactuated systems. In our case, $\eta_f \in [0.69, 0.99]$, and $\eta_m \in [0.72, 1]$ demonstrating minimal internal losses and high efficiency.

III. Haptic Device

The proposed haptic device allows the operator to control the vehicle's velocity or attitude rate sending reference to the onboard flight controller. The inertial frame $\mathcal{F}_C = \{O_C, \boldsymbol{x}_C, \boldsymbol{y}_C, \boldsymbol{z}_C\}$ with origin O_C corresponds to the idle orientation of the control sticks with $\boldsymbol{z}_R$ colinear to $\boldsymbol{z}_C$ (see Fig. 1). Their current poses are described by the frames $\mathcal{F}_L = \{O_L, \boldsymbol{x}_L, \boldsymbol{y}_L, \boldsymbol{z}_L\}$ and $\mathcal{F}_R = \{O_R, \boldsymbol{x}_R, \boldsymbol{y}_R, \boldsymbol{z}_R\}$ with respective origins O_L and O_R fixed with respect to the sticks.

The attitude and angular rates of $\mathcal{F}_L$ and $\mathcal{F}_R$ with respect to $\mathcal{F}_C$ are defined as $\boldsymbol{R}_L, \boldsymbol{R}_R \in \mathrm{SO}(3)$, and $\boldsymbol{\omega}_L, \boldsymbol{\omega}_R \in \mathbb{R}^2$, respectively, the latter expressed in $\mathcal{F}_L$ and $\mathcal{F}_R$.

The dynamic relation between the haptic sticks values are modeled in $\mathcal{F}_L$ and $\mathcal{F}_R$ as

$$\mathbf{M}_{fing} \begin{bmatrix} \dot{\boldsymbol{\omega}}_L \\ \dot{\boldsymbol{\omega}}_R \end{bmatrix} + \mathbf{D}_{fing} \begin{bmatrix} \boldsymbol{\omega}_L \\ \boldsymbol{\omega}_R \end{bmatrix} = \begin{bmatrix} -\boldsymbol{\tau}_{\mathrm{L}} \\ -\boldsymbol{\tau}_{\mathrm{R}} \end{bmatrix} + \begin{bmatrix} \boldsymbol{\tau}_{\mathrm{L,act}} \\ \boldsymbol{\tau}_{\mathrm{R,act}} \end{bmatrix}, \quad (5)$$

where $\boldsymbol{\tau}_{\mathrm{L,act}}, \boldsymbol{\tau}_{\mathrm{R,act}} \in \mathbb{R}^2$ represents the torques generated by the muscles and $\boldsymbol{\tau}_{\mathrm{L}}, \boldsymbol{\tau}_{\mathrm{R}} \in \mathbb{R}^2$ represents the interaction torque provided by the haptic device. The inherent inertia and damping properties of the human operator are $\mathbf{M}_{fing} \in \mathbb{R}^{4\times4}$ and $\mathbf{D}_{fing} \in \mathbb{R}^{4\times4}$.

A. Reference Generation

As it has been proposed in [12] for HHJ, we extend the reference generation to the HFJ kinematics. We use an admittance filter combined with a low-level joint position controller. This ensures a compliant interaction with the fingers and haptic transparency. Assuming perfect tracking of the joysticks, the closed-loop dynamics can be approximated as

$$\mathbf{M}_{adm} \begin{bmatrix} \dot{\boldsymbol{\omega}}_L \\ \dot{\boldsymbol{\omega}}_R \end{bmatrix} + \mathbf{D}_{adm} \begin{bmatrix} \boldsymbol{\omega}_L \\ \boldsymbol{\omega}_R \end{bmatrix} = \begin{bmatrix} -\boldsymbol{\tau}_{\mathrm{L}} \\ -\boldsymbol{\tau}_{\mathrm{R}} \end{bmatrix} + \boldsymbol{\tau}_{\mathrm{fb,total}}, \quad (6)$$

where $\mathbf{M}_{adm} = diag(\mathbf{M}_{adm,l}, \mathbf{M}_{adm,r}) \in \mathbb{R}^{4\times4}$ is the inertia and $\mathbf{D}_{adm} = diag(\mathbf{D}_{adm,l}, \mathbf{D}_{adm,r}) \in \mathbb{R}^{4\times4}$ is the damping coefficient. Both are determined by the user's preferences. While $\boldsymbol{\tau}_{\mathrm{fb,total}} \in \mathbb{R}^4$ is the feedback wrench applied to the operator.

We establish the connection between the constrained input workspace and the limitless operational space of the robot, with velocity control. This is a well-recognized method in teleoperating aerial vehicles [21]. We define $v_1, \omega_2 \in \mathbb{R}^3$ mapping orientations of the sticks $\boldsymbol{R}_R^C, \boldsymbol{R}_L^C \in \mathbb{R}^{3\times3}$ and orientation of the joystick body $\boldsymbol{R}_C^W$ into linear and angular velocities

$$v_1 = \mathbf{P}_{1L}\mathbf{Q}(\boldsymbol{R}_L) + \mathbf{P}_{1R}\mathbf{Q}(\boldsymbol{R}_R) + \mathbf{P}_{1C}\mathbf{Q}(\boldsymbol{R}_C), \quad (7a)$$

$$\omega_2 = \mathbf{P}_{2L}\mathbf{Q}(\boldsymbol{R}_L) + \mathbf{P}_{2R}\mathbf{Q}(\boldsymbol{R}_R) + \mathbf{P}_{2C}\mathbf{Q}(\boldsymbol{R}_C), \quad (7b)$$

with

$$\mathbf{Q}(\boldsymbol{R}) = \frac{(\boldsymbol{R} - \boldsymbol{R}^\top)^\vee}{\|(\boldsymbol{R} - \boldsymbol{R}^\top)^\vee\|}, \quad (8)$$

and where $\mathbf{P}_{1L}, \mathbf{P}_{1R}, \mathbf{P}_{1C}, \mathbf{P}_{2L}, \mathbf{P}_{2R}, \mathbf{P}_{2C} \in \mathbb{R}^{3\times3}$ are selection matrices defined by the control mode to map the 6-DoF joystick inputs to the 6-DoF capabilities of the omnidirectional platform. They are designed based on the control strategy and user preferences, each selecting relevant translational or rotational directions for a given joystick axis. An example in Sec. IV illustrates their implementation in a real-world teleoperation scenario. This design enables intuitive, decoupled control while respecting the platform's actuation limits. To map the finite stick workspace to the robot's potentially unbounded space, translational and rotational references are calculated such that

$$\boldsymbol{v}_{B,\mathrm{ref}} = \frac{v_{max}}{2}\, v_1, \quad (9a)$$

$$\boldsymbol{p}_{B,\mathrm{ref}} = \int_0^t \boldsymbol{v}_{B,\mathrm{ref}}(b)\, db, \quad (9b)$$

$$\boldsymbol{\omega}_{B,\mathrm{ref}}^B = \frac{\omega_{max}}{2}\, \omega_2, \quad (9c)$$

$$\boldsymbol{R}_{B,\mathrm{ref}}^W = \int_0^t \boldsymbol{R}_{B,\mathrm{ref}}^W(b)\, [\boldsymbol{\omega}_{B,ref}(b)]_\times\, db, \quad (9d)$$

where $(\cdot)_\times : \mathbb{R}^3 \mapsto so(3)$ is the skew-symmetric operator, while v_{max} and ω_{max} are, respectively, the maximum velocity and angular rate set by the operator preference.

B. Haptic Feedback Generation

As proposed in [12], we define the total feedback torque

$$\boldsymbol{\tau}_{\mathrm{fb,total}} = \boldsymbol{\tau}_{\mathrm{fb,rec}} + \boldsymbol{\tau}_{\mathrm{fb,ext}}, \quad (10)$$

where $\boldsymbol{\tau}_{\mathrm{fb,rec}} \in \mathbb{R}^4$ is the recentering torque of each stick and $\boldsymbol{\tau}_{\mathrm{fb,ext}} \in \mathbb{R}^4$ is the interaction torque. In detail

$$\boldsymbol{\tau}_{\mathrm{fb,rec}} = -\frac{\mathbf{K}_{rec}}{2} \begin{bmatrix} (\boldsymbol{R}_L^C - \boldsymbol{R}_L^{C\top})^\vee \\ (\boldsymbol{R}_R^C - \boldsymbol{R}_R^{C\top})^\vee \end{bmatrix}, \quad (11)$$

with $\mathbf{K}_{rec} = diag(\mathbf{K}_{rec,l}, \mathbf{K}_{rec,r}) \in \mathbb{R}^{4\times4}$ a tuning parameter. When the operator releases the stick, the recentering action causes it to return to the idle position, signifying a zero robot velocity. In other words, we replicate the mechanical spring and with frictions of current RC joysticks. An internal force-based impedance controller for each motor ensures modulation of force exertion. The torque feedback

during interaction is defined as $\boldsymbol{\tau}_{\text{fb,ext}} = \mathbf{K}_{ext}\hat{\boldsymbol{\tau}}_{\text{ext}}$, with $\mathbf{K}_{ext} \in \mathbb{R}^4$ a tuning parameter to adjust perceived effort to user preferences.

This modeling fits current teleoperation setups having conventional RC and has the potential to extend the device to more DoF per stick for overactuated systems. The formulation is independent of the device and allows the stick mapping of the four standard teleoperation control modes, known by Micro Aerial Vehicle (MAV) pilots.

C. Haptic Joystick Design

For miniaturization purposes, the electronics are tailored and composed of two custom electronic boards. The first board connects the smart servos and the Inertial Measurement Unit (IMU) to the second board. The last embeds the powering with the microcontroller unit. Both designs are open-source and shared on the GitHub[1] repository.

The joystick incorporates two servo motors per stick, generating a 4-DoF configuration. Four bearings ensure free rotation between the joystick lever and the internal coupling, with motion transmitted via a rigid metallic rod. Additionally, the joystick is equipped with an integrated IMU, featuring a 3-DoF accelerometer and a 3-DoF gyroscope. The attitude is estimated in quaternions and filtered using the Madgwick filter [22]. Following conversion to Euler angles, the rotations around the $\boldsymbol{x}_C$ and $\boldsymbol{y}_C$ axes are included in a custom data frame, which is transmitted via a serial link to the joystick driver. Additionally, the data frame includes the four axes of the two joysticks, represented by their respective orientations around the x and y axes relative to $\mathcal{F}_C$. The integration of these components into the joystick is illustrated in Fig. 3 as part of the system.

At powering the device, a control routine on the microcontroller manages communications with multi-threading. Both centering and external torques defined in Eq. (10) are mapped and computed internally with an impedance controller. The servo motors can reach up to 0.441 Nm, or 22 N force at the finger position on the sticks. It is more than ten times the baseline amplitude with 2 N in [15]. This high force feedback capability ensures operator immersion with a wide range of force rendering.

IV. Experimental Applications

For this first application, the operator controls the aerial robot in translational velocities with the sticks in standardized for teleoperators $mode - 2$ configuration. In addition, the orientation around $\boldsymbol{x}_C$ and $\boldsymbol{y}_C$ are mapped to the robot attitude in roll and pitch. In Eq. (7), the matrices $\mathbf{P}_{1L}, \mathbf{P}_{1R}, \mathbf{P}_{1C}, \mathbf{P}_{2L}, \mathbf{P}_{2R}, \mathbf{P}_{2C}$ are sparse matrices where only the following elements are equal to one: $\{(\mathbf{P}_{1L})_{3,2}, (\mathbf{P}_{2L})_{1,2}, (\mathbf{P}_{2L})_{2,1}, (\mathbf{P}_{1R})_{3,1}, (\mathbf{P}_{2C})_{1,2}, (\mathbf{P}_{2C})_{2,1}\}$, and zero otherwise.

The proposed telemanipulation system is composed of the haptic joystick and the omnidirectional robot. The platform presented in Sec. II uses PX4 [23] FC both for the real platform and the SITL. Modifications to integrate the controller and the haptic RC are shared in the Github[2] repository. The haptic device detailed in Sec. III links the platform through bilateral communication in ROS2. Fig. 3 illustrates the whole architecture.

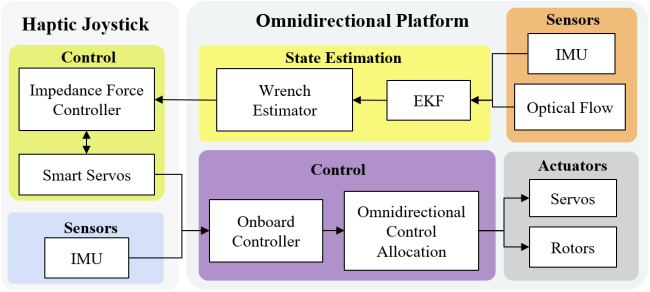

Fig. 3: Interaction of telemanipulation system components.

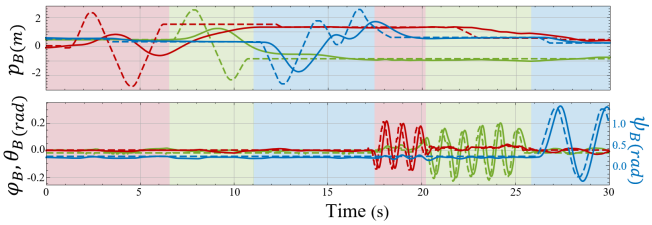

Fig. 4: Illustration of single axis generation in dotted line, highlighted with shaded color. The robot state in plain line.

A. Single Axis Reference Generation

Steering the vehicle in a single DoF is a key feature of the system. It simplifies control, enhancing precision for APhI and maneuverability in complex industrial environments. To evaluate reference generation from the haptic device, we use SITL within a physics engine simulator [24], which connects all hardware components and simulates the environment and sensor noise. For each axis, we perform 30 s back-and-forth motions and assess the statistical influence on the other axes. Fig. 4 shows that motion along one axis does not significantly affect the others. The full experiment is summarized in Table II, reporting the Mean Absolute Error (MAE) of each reference axis relative to the others.

TABLE II: MAE of repetitive axis command *(column)* with respect to other axis *(row)*.

	$\dot{x}_B$	$\dot{y}_B$	$\dot{z}_B$	$\dot{\phi}_B$	$\dot{\theta}_B$	$\dot{\psi}_B$
$\dot{x}_B$	×	0.04048	0.0580	0.00021	0.00023	0.0023
$\dot{y}_B$	0.258	×	0.023	0.0007	0.0021	0.0061
$\dot{z}_B$	0.0737	0.0302	×	0.00876	0.0213	0.00246
$\dot{\phi}_B$	0.0360	0.0417	0.2270	×	0.0599	0.0078
$\dot{\theta}_B$	0.0217	0.1010	0.0142	0.0126	×	0.1032
$\dot{\psi}_B$	0.0258	0.0596	0.1079	0.0020	0.0338	×

Overall, the table indicates that the influence of one axis on the others is generally low, with MAE values remaining close to zero. Although minor perturbations are observed, such as $\dot{x}_B$ when commanding $\dot{y}_B$ (0.258) or on $\dot{z}_B$ when

[2]https://github.com/tilties2/PX4-OmniQuad.git

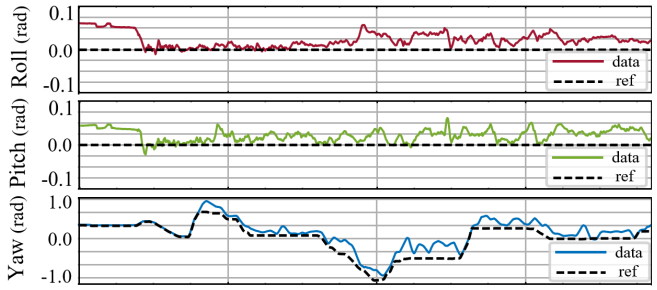

(a) Attitude tracking performance with command reference.

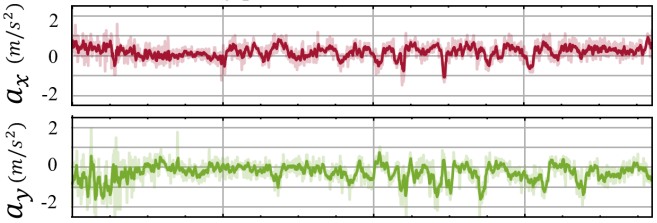

(b) Measured acceleration from onboard inertial sensing.

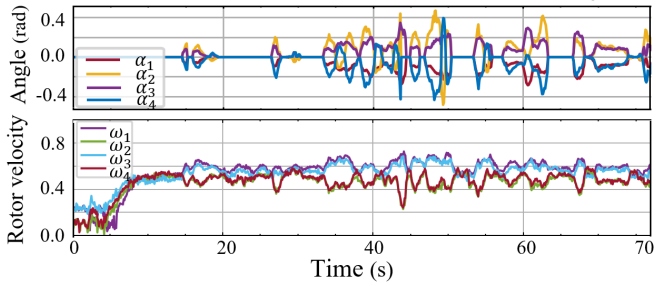

(c) Servo angle state (top) and rotors normalized speed (bottom) during flight test.

Fig. 5: Flight test result performances of the omnidirectional aerial robot in free flight.

commanding $\dot{\phi}_B$ (0.2270), these are not significant. The data suggest that the axes are largely decoupled, and the system exhibits good independent control with only minor perturbations between axes.

By keeping the conventional RC form factor, our haptic device resolved the coupling of rotational reference with translational references observed in [12] and [14]. The explanation comes from the physical decoupling of each stick. However, axes that are coupled in pairs also have little effect. Thus, the proposed device should be considered for future aerial telemanipulation applications.

B. Preliminary Flight Tests

To evaluate the flight capabilities of the system, we perform two preliminary stable flights. In the first one, we make freeflight in horizontal attitude. In other words, we want to command the platform in pure translations and yaw. As a result, the platform is capable of quickly translating in the plane $(O_B, \boldsymbol{x}_W, \boldsymbol{y}_W)$, as shown by its acceleration values (Fig. 5b), while maintaining a horizontal orientation relative to the ground. In particular, the measured roll and pitch of the platform (Fig. 5a) remain close to zero for the entire flight. The measured roll average angle is 0.026 rad while the pitch is 0.021 rad. Regarding its actuation capability, the

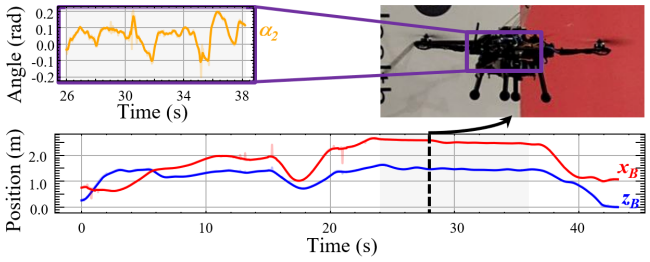

Fig. 6: Plot of the robot navigation mission in the plane $(O_W, \boldsymbol{x}_W, \boldsymbol{z}_W)$ with a physical interaction shaded in grey. During the contact, we plot the rotor angle α_2.

servo angles and the rotor command are shown in Fig. 5c. We observe continuous variations of the four servo angles to match the desired forces (Fig. 5c). A slight difference between the rotor speed (Fig. 5c) of the first and third rotor with respect to the second and fourth rotor is noticeable at around 40 s. It is a consequence of the decrease in the desired yaw (Fig. 5a). Then the rotor speeds consistently stay within 40% to 60% of their maximum value, with an average of 48.3%, demonstrating an efficient lift-to-mass ratio for the platform, as well as a good output of the proposed allocation matrix (Eq. (4)).

The last experiment consists of going into contact and pushing against a vertical wall to show stable interaction and tilting capabilities of the aerial vehicle. When the drone begins contact, vertical oscillations can be observed in Fig. 6 before stabilization at $t = 30$ s by continuing to push. During the 12 s duration of the physical interaction, α_1 had an average of 0.05 rad showing an overall push in the robot's forward direction. Some negative angles are still noticeable while the drone keeps contact. This can be explained by the overall internal force that is compensated by other rotors, which brings even more stability to the flying machine.

V. Conclusion

By integrating a miniaturized haptic device into a conventional RC shape with HFJ, we resolved the problem of coupling rotation and translation motion of omnidirectional multirotor. The proposed platform mechanical design allows us to reach state-of-the-art full actuation flight performance, while improving thrust-to-weight ratio and simplifying platform maintenance. All components of this system, both hardware and software, are open-sourced, making it accessible and modular for the wider research and development community in practical applications. The presented system sets new opportunities for omnidirectional drone control, providing a highly efficient and user-friendly solution. Future works will extend the generalized teleoperation framework to enable the control and mapping of additional DoF. In particular, our aim is to provide the operator with control over the robot's internal forces. This would enhance platform stability, while we would question how to deliver feedback on the internal state through haptic modalities.

REFERENCES

[1] A. Ollero, M. Tognon, A. Suarez, D. Lee, and A. Franchi, "Past, present, and future of aerial robotic manipulators," *IEEE Transactions on Robotics*, vol. 38, no. 1, pp. 626–645, 2022.

[2] M. Selvaggio, M. Cognetti, S. Nikolaidis, S. Ivaldi, and B. Siciliano, "Autonomy in physical human-robot interaction: A brief survey," *IEEE Robotics and Automation Letters*, vol. 6, no. 4, pp. 7989–7996, 2021.

[3] A. Kanso, I. H. Elhajj, E. Shammas, and D. Asmar, "Enhanced teleoperation of uavs with haptic feedback," in *2015 IEEE International Conference on Advanced Intelligent Mechatronics (AIM)*, 2015, pp. 305–310.

[4] K. Bodie, M. Brunner, M. Pantic, S. Walser, P. Pfändler, U. Angst, R. Siegwart, and J. Nieto, "Active interaction force control for contact-based inspection with a fully actuated aerial vehicle," *IEEE Transactions on Robotics*, vol. 37, no. 3, pp. 709–722, 2020.

[5] P. Zheng, X. Tan, B. B. Kocer, E. Yang, and M. Kovac, "Tiltdrone: A fully-actuated tilting quadrotor platform," *IEEE Robotics and Automation Letters*, vol. 5, no. 4, pp. 6845–6852, 2020.

[6] H. Zhong, J. Liang, Y. Chen, H. Zhang, J. Mao, and Y. Wang, "Prototype, modeling, and control of aerial robots with physical interaction: A review," *IEEE Transactions on Automation Science and Engineering*, 2024.

[7] B. Xu, F. Gao, C. Yu, R. Zhang, Y. Wu, and Y. Wang, "Omnidrones: An efficient and flexible platform for reinforcement learning in drone control," *IEEE Robotics and Automation Letters*, vol. 9, no. 3, pp. 2838–2844, 2024.

[8] C. Rognon, V. Ramachandran, A. R. Wu, A. J. Ijspeert, and D. Floreano, "Haptic feedback perception and learning with cable-driven guidance in exosuit teleoperation of a simulated drone," *IEEE Transactions on Haptics*, vol. 12, no. 3, pp. 375–385, 2019.

[9] M. Aggravi, C. Pacchierotti, and P. R. Giordano, "Connectivity-maintenance teleoperation of a uav fleet with wearable haptic feedback," *IEEE Transactions on Automation Science and Engineering*, vol. 18, no. 3, pp. 1243–1262, 2021.

[10] H. Courtois and N. Aouf, "Haptic feedback for obstacle avoidance applied to unmanned aerial vehicles," in *2017 International Conference on Unmanned Aircraft Systems (ICUAS)*, 2017, pp. 417–424.

[11] A. Y. Mersha, S. Stramigioli, and R. Carloni, "On bilateral teleoperation of aerial robots," *IEEE Transactions on Robotics*, vol. 30, no. 1, pp. 258–274, 2014.

[12] M. Allenspach, N. Lawrance, M. Tognon, and R. Siegwart, "Towards 6dof bilateral teleoperation of an omnidirectional aerial vehicle for aerial physical interaction," in *2022 International Conference on Robotics and Automation (ICRA)*, 2022, pp. 9302–9308.

[13] J. Mellet, M. Allenspach, E. Cuniato, C. Pacchierotti, R. Siegwart, and M. Tognon, "Evaluation of human-robot interfaces based on 2d/3d visual and haptic feedback for aerial manipulation," *arXiv preprint arXiv:2410.15398*, 2024.

[14] M. Young, C. Miller, Y. Bi, W. Chen, and B. D. Argall, "Formalized task characterization for human-robot autonomy allocation," in *2019 International Conference on Robotics and Automation (ICRA)*, 2019, pp. 6044–6050.

[15] S. Mintchev, M. Salerno, A. Cherpillod, S. Scaduto, and J. Paik, "A portable three-degrees-of-freedom force feedback origami robot for human–robot interactions," *Nature Machine Intelligence*, vol. 1, no. 12, pp. 584–593, 2019.

[16] M. Brunner, G. Rizzi, M. Studiger, R. Siegwart, and M. Tognon, "A planning-and-control framework for aerial manipulation of articulated objects," *IEEE Robotics and Automation Letters*, vol. 7, no. 4, pp. 10 689–10 696, 2022.

[17] M. Kamel, S. Verling, O. Elkhatib, C. Sprecher, P. Wulkop, Z. Taylor, R. Siegwart, and I. Gilitschenski, "Voliro: An omnidirectional hexacopter with tiltable rotors," *arXiv*, 2018.

[18] T. Hui, E. Cuniato, M. Pantic, M. Tognon, M. Fumagalli, and R. Siegwart, "Passive aligning physical interaction of fully-actuated aerial vehicles for pushing tasks," 2024. [Online]. Available: https://arxiv.org/abs/2402.17434

[19] F. Buonamici, M. Carfagni, R. Furferi, Y. Volpe, L. Governi *et al.*, "Generative design: an explorative study," *Computer-Aided Design and Applications*, vol. 18, no. 1, pp. 144–155, 2020.

[20] M. Allenspach, K. Bodie, M. Brunner, L. Rinsoz, Z. Taylor, M. Kamel, R. Siegwart, and J. Nieto, "Design and optimal control of a tiltrotor micro-aerial vehicle for efficient omnidirectional flight," *The International Journal of Robotics Research*, vol. 39, no. 10-11, pp. 1305–1325, 2020.

[21] F. Conti and O. Khatib, "Spanning large workspaces using small haptic devices," in *First Joint Eurohaptics Conference and Symposium on Haptic Interfaces for Virtual Environment and Teleoperator Systems. World Haptics Conference*, 2005, pp. 183–188.

[22] S. Madgwick *et al.*, "An efficient orientation filter for inertial and inertial/magnetic sensor arrays," *Report x-io and University of Bristol (UK)*, vol. 25, pp. 113–118, 2010.

[23] S. Marcellini, J. Cacace, and V. Lippiello, "A px4 integrated framework for modeling and controlling multicopters with til table rotors," in *2023 International Conference on Unmanned Aircraft Systems (ICUAS)*. IEEE, 2023, pp. 1089–1096.

[24] R. Smith, "Open Dynamics Engine," 2008, http://www.ode.org/.